Journal of Materials Chemistry B

Porous nanozymes: peroxidase-mimetic activity of mesoporous iron oxide for colorimetric and electrochemical detection of global DNA methylation

Journal:	*Journal of Materials Chemistry B*
Manuscript ID	TB-ART-04-2018-001132.R1
Article Type:	Paper
Date Submitted by the Author:	12-Jun-2018
Complete List of Authors:	Bhattacharjee, Ripon ; Griffith University Nathan Campus, Natural Science Tanaka, Shunsuke; University of Wollongong Moriam, Sofia; Griffith University, School of Natural Sciences Masud, Mostafa Kamal; Griffith University, Queensland Micro- and Nanotechnology Centre; Shahjalal University of Science and Technology School of Life Sciences, Biochemistry and Molecular Biology Lin, Jianjian; Nanjing Tech University, Institute of Advanced Materials Alshehri, Saad; King Saud University, Chemistry Ahamad, Tansir; King Saud University, Chemistry Salunkhe, Rahul; Hanyang University, Department of Organic and Nano Engineering Nguyen, Nam-Trung; Griffith University, Queensland Micro- and Nanotechnology Centre Yamauchi, Yusuke; University of Queensland Australian Institute for Bioengineering and Nanotechnology, ; National Institute for Materials Science, WPI Center for MANA Hossain, Md Shahriar; University of Wollongong, Australian Institute for Innovative Materials Shiddiky, Muhammad; Griffith University (Nathan Campus), School of Natural Sciences

TOC Text

Peroxidase-mimetic activity of mesoporous Fe_2O_3 nanomaterials in global DNA methylation detection using naked eye and electrochemical readout.

TOC Graphic

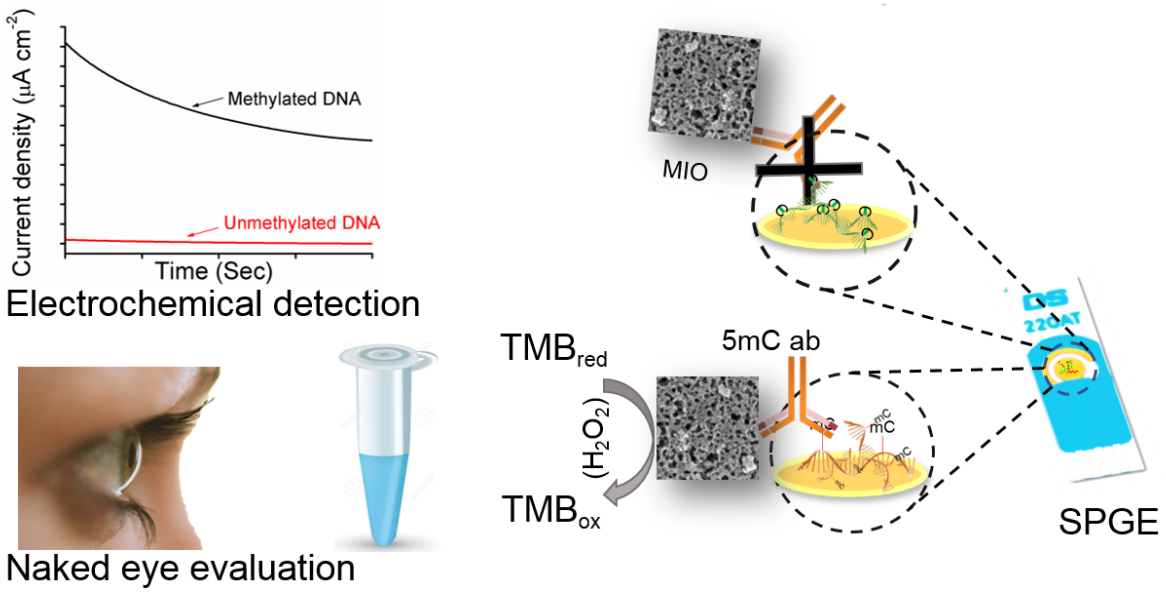

Porous nanozymes: peroxidase-mimetic activity of mesoporous iron oxide for colorimetric and electrochemical detection of global DNA methylation

Ripon Bhattacharjee,[a] Shunsuke Tanaka,[b,c] Sofia Moriam,[a] Mostafa Kamal Masud,[a,c] Jianjian Lin,[b,c] Saad M. Alshehri,[d] Tansir Ahamad,[d] Rahul R. Salunkhe,[e] Nam-Trung Nguyen,[a] Yusuke Yamauchi,[f,g]* Md. Shahriar A. Hossain,[c,f]* and Muhammad J. A. Shiddiky[a]*

[a] School of Environment and Science & Queensland Micro- and Nanotechnology Centre (QMNC), Griffith University, Nathan Campus, Nathan, QLD 4111, Australia

[b] College of Chemistry and Molecular Engineering, Qingdao University of Science and Technology, Qingdao 266042, China

[c] Australian Institute for Innovative Materials (AIIM), University of Wollongong, Squires Way, North Wollongong, NSW 2500, Australia

[d] Department of Chemistry, College of Science, King Saud University, Riyadh 11451, Saudi Arabia.

[e] International Centre for Materials Nanoarchitectonics (MANA), National Institute for Materials Science (NIMS), 1-1 Namiki, Tsukuba, Ibaraki 305-0044, Japan.

[f] School of Chemical Engineering, School of Mechanical and Mining Engineering, and Australian Institute for Bioengineering and Nanotechnology (AIBN), The University of Queensland, Brisbane, QLD 4072, Australia

[g] Department of Plant & Environmental New Resources, Kyung Hee University, 1732 Deogyeong-daero, Giheunggu, Yongin-si, Gyeonggi-do 446-701, South Korea

*Corresponding author e-mails:

y.yamauchi@uq.edu.au; md.hossain@uq.edu.au; m.shiddiky@griffith.edu.au

† Electronic supplementary information (ESI) available.

Abstract

The peroxidase-mimetics of nanomaterials (nanozymes) have widely been used in biosensing platform as low-cost, relatively stable and prevailing alternatives to natural enzymes. Herein, we report on the synthesis and application of peroxidase-mimetic activity of mesoporous iron oxides (MIO) for the detection of global DNA methylation in colorectal cancer cell lines. The target DNA were extracted and denatured to get ssDNA followed by the direct adsorption onto the surface of a bare screen-printed gold electrode (SPGE). 5-methyl cytosine antibody (5mC) functionalized nanomaterial (MIO-5mC) were then used to recognise the methylcytosine groups present on the SPGE. The MIO-5mC conjugates catalyse the TMB solution in the presence of the hydrogen peroxide to give the colorimetric (i.e., naked-eye observation) and electrochemical detection of DNA methylation. The assay could successfully detect as low as 10% difference of global DNA methylation level in synthetic samples and cell lines with good reproducibility and specificity (% RSD = <5%, for n = 3). This strategy avoids the use of natural enzyme horseradish peroxidase (HRP), traditional PCR based amplification and bisulfite treatment steps that have generally been used in many conventional DNA methylation assays. We envisage that our assay could be a highly potential low-cost platform for genome-wide DNA methylation analysis in point-of-care applications.

Keywords: mesoporous iron oxides, nanobiotechnology, peroxidase-like activity, global DNA methylation, colorimetric, and electrochemical detection.

1. Introduction

With the remarkable advancements of nanotechnology, nanostructured metal nanoparticles (NPs) have aroused immense attention in the field of nanobiotechnology, analytical sensing, catalysis, and nanomedicine. [1] Among all NPs, iron oxide NPs have considered as promising materials for biosensing application as they possess low toxicity, excellent biocompatibility, super-paramagnetism, high thermal and chemical stability and relatively easy bio-functionalization (due to superior affinity to different organic and polymeric linkers). [2-4] It has been shown that iron oxide NPs possess intrinsic enzyme-like (e.g., HRP) activity towards the oxidation of enzyme substrates such as 3,3′,5,5′-tertamethylbenzidine (TMB), o-phenylenediamine (OPD), diazoaminobenzene (DAAB). [5] Moreover, iron oxide NPs possess superior benefits over HRP in many biological and environmental sensing application owing to their robustness, inexpensive and easy synthesis and therefore, considered as an alternative of HRP in sensing platform. [6-8] Using peroxidase mimetics of iron oxide NPs, several sensors have been developed for biomolecular detection. [6, 9] However, most of the reported nanomaterials demonstrate their peroxidase-like activity at a higher temperature (40−45°C), which substantially limits their applications in the development of biosensors for disease-specific biomarker at room temperature. Therefore, NPs with superior peroxidase-mimetics at room temperature are highly demanding for sensitive biomolecule sensing. Nanoengineered morphology such as nanoporous structure could give higher peroxidase-mimetics at room temperature as porous structure significantly enhances the surface to volume ratio for up-taking higher amount of analytes or redox molecules, and strengthen the activity and selectivity of catalytic reactions by offering sequential catalytic compartments and stabilization of substrate from sintering. [10-12] In this report we have enginered a mesoporous Fe_2O_3, which shows excellent peroxidase-mimetics at room temperature.

DNA methylation is one of the key epigenetic marks, where methylation occur at a cytosine (C5 position) base of DNA in cytosine/guanine (CpG) dinucleotides sites mostly located in the promoter regions of mammalian genes. [13] Aberrancies in methylation are responsible for cancer pathogenesis *via* dysregulation of various cellular pathways including genomic stability, chromatin modulation, transcription of proto-oncogenes, and activation of tumour suppressor genes. [14, 15] For instance, colorectal adenomas or adenocarcinomas have a strong correlation between the malignant phenotype and DNA methylation status. Therefore, a sensitive platform for global methylation detection of colorectal cancer is very crucial to reduce the colorectal cancer associated burden as well as death. Over the last few decades, several strategies such as high-performance liquid chromatography (HPLC), tandem mass spectrometry (LC-MS/MS), high-performance capillary electrophoresis, and bisulfite modification of DNA followed by some form of sequencing have been reported for the detection of global DNA methylation. [16, 17, 18] Although most of the methods are highly quantitative and reproducible, they are limited from the requirements of relatively large amounts of DNA, sophisticated instruments, and time-consuming assay optimization. Though PCR based methods such as pyrosequencing and methylation-sensitive restriction methods usually entailed less amount of DNA, but they involved time-consuming and laborious bisulfite conversation, expensive restriction enzymes (e.g., MspI and HpaII) and limited to DNA methylation analysis of specific sequences. [19] In recent time, numerous colorimetric [20] and electrochemistry [21] based assays have also been developed for DNA methylation analysis. On the other hand, electrochemical detection has its inherent advantages of fast, high specificity, sensitivity, and compatibility with multiplexing and miniaturization. [20, 22] Therefore, a combined platform consisting of both methods could be useful for achieving sensitive and accurate DNA methylation analysis. Previously, we [23] and other groups [10] have coupled these two detection methods for analysing DNA methylation in clinical samples. In

these assays, HRP conjugated 5mC antibody or methyl-CpG-binding domain (MBD) proteins have been used to specifically recognize the methylated sites present in the target DNA. Although these methods have better analytical performances in terms of specificity and sensitivity, they rely on HRP-based enzymatic reactions. Nowadays, NPs (peroxidase-mimetics) have interrogated in such biosensors for obtaining greater sensitivity and an excellent alternative to HRP. [6] To the best of our knowledge, peroxidase-mimetics of mesoporous iron oxides have never been used in DNA methylation analysis.

In this assay, we have integrated peroxidase-mimetics of an in-house synthesized MIO for the development of a colorimetric and electrochemical platform for DNA methylation detection. The assay involves several steps; *i)* functionalization of MIO with 5mC antibody (MIO-5mC conjugates), *ii)* direct adsorption of extracted and denatured ssDNA (from colorectal cancer cell lines) on to a bare gold electrode surface, *iii)* recognition of methylated sites using MIO-5mC conjugates and *iv)* surface attached MIO (*via* specific interaction between methylation sites and 5mC antibody of MIO-5mC conjugates) catalized oxidation of TMB in the presence of H_2O_2 to generate the corresponding signals. The signal (color change) was observed and quantified by using colorimetry and chrono-amperometry (*i*-*t*).

2. Experimental

2.1 Reagents and chemicals

Poly (ethylene glycol) methyl ether (4-cyano-4-pentanoate dodecyl trithiocarbonate) was purchased from Sigma Aldrich (Japan). PEG-CTA and 2,2'-azobis (2,4-dimethyl valeronitrile) were purchased from Wako Pure Chemicals (Japan) and were used without further purification. 2,2'-Azobis (isobutyronitrile) (AIBN) obtained from Wako Pure

Chemicals and was recrystallized from methanol prior to use.1,4-Dioxane and acrylic acid (AA, > 98.0%) and styrene (> 99.0%) was purchased from Wako Pure Chemicals and further dried and purified before applying for synthesis. Tetrahydrofuran (THF), iron(III) nitrate nonahydrate ($Fe(NO_3)_3 \cdot 9H_2O$, 99.99%), sodium hydroxide (NaOH, 99.9%), and ethanol (99.5%) were purchased from Nacalai Tesque (Japan). UltraPure DNase/RNase-free distilled water was obtained from Invitrogen (Carlsbad, CA, USA). Screen printed gold electrode (SPGE) (220BT; diameter = 4 mm) consisting three-electrode system (printed on a ceramic substrate) were acquired from Dropsens (Asturias, Spain).

2.2 Synthesis of mesoporous iron oxide

We have synthesized mesostructured iron oxide using polymeric micelles following our recent report. [24] To keep a significant amount of carbon content in the final product, we intentionally calcined the as-prepared mesostructured material at relatively lower temperature than usual. Here mesostructured iron oxide were calcined in air at 350 °C for 4 h, with a heating rate of 1 $°Cmin^{-1}$ to obtain the mesoporous iron oxide.

2.3 Mesoporous iron oxide characterization

The morphological observations of the mesoporous iron oxide sample was conducted using scanning electron microscope (SEM) (Hitachi SU-8000) operated at an accelerating voltage of 10 kV and transmission electron microscope (TEM) (JEOL JEM-2100F) operated at an accelerating voltage of 200 kV. The surface composition of the samples was analyzed using X-ray photoelectron spectroscopy (XPS) with a PHI Quantera SXM (ULVAC-PHI) instrument using an Al-Kα X-ray source.

2.4 Peroxidase-mimetics kinetics

The peroxidase-like activities of the mesoporous Fe_2O_3 was investigated through the catalytic oxidation of TMB in the presence of H_2O_2 to produce a blue color charge trannsfer complex. TMB substrate solution was prepared in 0.2M sodium acetate (NaAc) buffer (pH 3.5) using 800 μM freshly prepared TMB (TMB dissolved in DMSO) and 700 mM H_2O_2. The formation of blue colored solution was monitored and measured at 652 using a spectrophotometer (SpectraMax). The reaction (formation of blue colored complex) was quenched by adding 2.0 μL of stop solution (2.0 M HCl), which gave a yellow colored product. Colorimetry (at 452 nm) was used to measure the intensity of resultant yellow color product and chroamperometric measurement was done at +150 mV to obtain the corresponding electrochemical signals at 60 s.

The steady-state kinetic experiments were performed using 5μg of MIO for both TMB and H_2O_2 as a substrate. The H_2O_2 concentration were kept constant (700 mM) while the concentration of TMB was varied ranging from 0.01-1.0 mM. Similarly, the kinetics with H_2O_2 as the substrate was performed using identical amount of MIO with fixed concentration of TMB (800 μM) and varying concentration of H_2O_2 (0.01-1.0 M). A typical enzyme catalysis reaction can be considered to represent this reaction mechanism;

$$E + S \underset{K_{-1}}{\overset{K_1}{\rightleftharpoons}} ES \xrightarrow{K_2} E + P \quad \ldots \quad \ldots \quad (1)$$

Here E, S, ES and P are defined as the enzyme (Fe_2O_3), substrate (TMB/H_2O_2), enzyme-substrate complex and product, respectively. Kinetic parameters were estimated based on the Michaelis–Menten equation and Line weaver-Burk equation.[25]

$$V = V_{max} \frac{[S]}{[S] + K_m} \quad \ldots \quad \ldots \quad \ldots \ldots \ldots \quad (2)$$

In this equation, V is the rate of conversion (velocity) V_{max} is the maximum rate of conversion, [S] is the substrate concentration, and K_m is the Michaelis constant which is equivalent to the substrate concentration at which the rate of conversion is half of $V_{max.}$ K_m denotes the affinity of the enzyme for the substrate. The rearrangement of equation (2) give rise to the Line weaver-Burk equation to calculate the enzyme kinetics terms K_m and V_{max}.

$$\frac{1}{V} = \frac{K_m}{V_{max}} \frac{1}{[S]} + \frac{K_m}{V_{max}} \quad \ldots \quad \ldots \quad \ldots \quad (3)$$

2.5 Isolation and purification of genomic DNA

Two colorectal cancer cell lines (HCT-116, SW-48) and one normal cell line (FHC-N) were purchased from American Type Culture Collection (ATCC), USA. A blood and cell culture DNA mini kit (Qiagen, Hilden, Germany) was used to extract and purify the DNA from these cell lines. Jurkat (100% methylated) and whole genomic amplified DNA (WGA) kit were purchased from New England BioLab. Genomic DNA were denatured at 95 ^{o}C for 10 mins to get the single strand DNA. Whole genome amplification DNA was prepared by following the protocol of REPLI-g whole genome amplification mini kit (Qiagen, Hilden, Germany) and purified following the protocol DNeasy Blood & Tissue Kits (Qiagen).

2.6 Preparation of iron oxide conjugated antibody

Prior to conjugation of porous Fe_2O_3 with 5mC antibody, the MIO was first functionalized with dextran following previously published articles.[5, 26, 27] In brief, 10 µl of 2 mg/ml dextran (prepared in 0.5M NaOH solution) and 10 µl of 10 µg/µl MIO was thoroughly mixed and

incubated at room temperature in a thermomixer (300 rpm). After the overnight incubation, the MIO was separated from unbound dextran using an external magnet. In order to couple the antibody, 20 µl (2 mg/ml) $NaIO_4$ solution were added into the dextran-modified MIO followed by 20 min incubation at 37 ^oC. The conjugates were washed three times with 0.2 M NaAc (pH 4.5). The activated MIO was then added and incubated with 75 ng/µl antibody at 4 ^oC overnight. $NaBH_4$ was then used to stop the coupling reaction. The MIO-5mC antibody conjugates were washed with PBS and isolated using an external magnet. Finally, PBS was added to obtain 200 ng/µl MIO-5mC antibody conjugates and stored at 4 ^oC for conducting the subsequent experiments. As dextran is a branched polysaccharide comprised of glucose subunits, polar interactions (chelation and hydrogen bonding) allow it to covalently bind with the carbohydrate site of the 5mC antibody. [28] In this conjugation process, strong alkaline solution was used to get stable aggregation of Fe_2O_3 and dextran. [27] The oxidizing agent, $NaIO_4$ was used to create numerous aldehyde residues sites at dextran thus it can easily bind to amine site of antibody protein *via* Schiff base interactions. [29] Finally, reduction agents $NaBH_4$ terminate the coupling reaction and form a stable Fe_2O_3 conjugated 5mC antibody. The use of $NaBH_4$ also improved the nanoparticle activity by increasing the Fe^{2+} ions in the reaction system. [30] To demonstrate the successful conjugation of porous Fe_2O_3 with 5mC antibody, we have taken UV-vis absorption spectra for the samples with MIO, dextran- and dextran/5-mC antibody-modified MIO (Fig. S2). A small bathochromic shift of the peak at around 360 nm and increase in the absorbance value with the addition of dextran (red) and antibodies (blue) indicating their successful conjugation with MIO.[31, 32]

2.8 Colorimetric and electrochemical detection of global DNA methylation

20 μL of isolated genomic DNA were denatured at 95 ^{o}C followed by the dilution with 5x saline sodium citrate (SSC) buffer to obtain 10 ng/μL of ssDNA. 5 μL of denatured ssDNA samples were then dropped onto a screen-printed gold electrode (SPGE) surface and allowed to adsorb for 10 min. 5 μL of MIO-5mC antibody (200 ng/μL) was then added onto the gold electrode surface and allowed to incubation for 30 min at room temperature with gentle shaking (unless otherwise stated) to facilitate the binding of the MIO-5mC antibody conjugate with the designated methyl cytosine site of ssDNA. After the incubation, the electrode was washed with 10 mM PBS (pH 7.4) to remove loosely bound or unbounded MIO-5mC antibody conjugates. To obtain the colorimetric responses, 60 μL of freshly prepared TMB substrate solution was added onto the gold electrode surface and incubated in the dark at room temperature for 10 min. The MIO of DNA bounded MIO-5mC antibody conjugates catalysed the TMB reaction in the presence of H_2O_2 and generated a blue color charge-transfer complex solution. The corresponding color change facilitates the naked-eye observation of global DNA methylation. The amount of MIO catalysed oxidation (the intensity of the generated color) was quantified after the addition of 2 μL of 2.0 M HCl. The absorbance of developed yellow color was measured at 452 nm using an ultra-violet (UV)-visible spectrophotometer. The TMB_{ox} product is electro-active which offers the electrochemical quantification of biorecognition events. [33] To perform electrochemical measurements, a CH1040C potentiostat (CH Instruments, TX, USA) was used. Chronoamperometric measurements were conducted by placing 50 μL of yellow solution (TMB oxidized product) onto a cleaned SPGE surface with a potential of +150 mV. The current levels generated at 40 seconds were used for quantitative analysis. At least three replicates were measured for each standard/sample and all data were subtracted from the background data. All measurements were performed at room temperature.

2.9 Determination of the Surface Area of the Electrodes

The effective working area of the electrodes was calculated by measuring the peak current obtained as a function of scan rate under cyclic voltammetric conditions for the one-electron reduction of $[Fe(CN)_6]^{3-}$ [2.0 mM in PBS (0.5 M KCl)] and by using the Randles-Sevcik equation (equation 4),

$$i_p = (2.69 \times 10^5) n^{3/2} A D^{1/2} C v^{1/2} \quad \ldots\ldots\ldots\ldots\ldots (4)$$

where, ip is the peak current (A), n is the number of electrons transferred ($Fe^{3+} \rightarrow Fe^{2+}$, n = 1), A is the active area of the electrode (cm^2), D is the diffusion coefficient of $[Fe(CN)_6]^{3-}$ taken to be 7.60 × 10-5cm^2s^{-1}), C is the concentration (mol cm^{-3}), ν is the scan rate (Vs^{-1}).

3. Results and discussion

3.1 Characterization of mesoporous iron oxide

The surface morphology of the as-prepared mesoporous iron oxide was observed using scanning electron microscope (SEM) images and transmission electron microscope (TEM). SEM and TEM images (Fig. 1(A), (B)) shown the mesoporous structure of as synthesized iron oxide. The carbon contents of block copolymer still remain on the surface of the sample since the calcination temperature is not high enough to remove template. [24] The selected area electron diffraction (SAED) patterns demonstrate polycrystalline nature of γ-Fe_2O_3 in the pore walls (Fig. 1(C). From the high resolution TEM image, clear lattice fringes with a *d*-spacing of 0.29 nm were confirmed, which corresponds to (220) plane of γ-Fe_2O_3 crystal (Fig. 1(D)).[34]

The surface composition of the mesoporous iron oxide calcined at 350 ^{0}C was analyzed by XPS analysis, as shown in Fig. S1. The presence of Fe, O, and C elements was

confirmed by the survey spectrum. (Fig. S1 (A)) The atomic percentages of Fe, O and C by XPS are 2.9, 27.5 and 69.6 atomic %. The presence of a large amount of carbon originated from the remaining carbon from the used block polymer. The deconvoluted peaks of C1s can be indexed to C=C, C-O, and C=O bonds of the remaining block copolymer (Fig. S1 (B)). The deconvoluted peaks of O1s appears at 530 eV are attributed to typical metal oxide. (Fig. S1 (C)) The other peaks correspond to C-O and O-H bonds and adsorbed water. [35] The deconvoluted peaks of Fe2p at binding energy 710 eV and 724 eV with satellite peaks correspond to Fe $2p_{3/2}$ and Fe $2p_{1/2}$, indicating the formation of Fe^{3+} (Fig. S1 (D)). [36] Fe^0 and Fe^{2+} were not detected, indicating that the obtained mesoporous iron oxide is Fe_2O_3.

3.2 Peroxidase mimetic activity of mesoporous Fe_2O_3

To investigate the peroxidase mimetic activity of MIO, we used as synthesized porous Fe_2O_3 particle to oxidise TMB substrate solution and measured the absorbance of generated color. It has been well known that, natural peroxidase (HRP) can catalyse the TMB in the presence of H_2O_2 and generate a blue color charge-transfer complex. We observed that our mesoporous Fe_2O_3 possessed significant peroxidase-like activity at room temperature. We investigated the peroxidase mimetic activity of the MIO following our previously published articles. [3, 37] In brief, two control experiments were carried out where with MIO was taken as positive and without MIO was as negative control. About 40 times higher intensity was observed for the positive control compare to that of negative control (0.56 vs. 0.014, abs@452nm) (Fig. 2A). After the addition of 2.0 M HCl, blue color solution (charge transfer complex) turns to yellow colored diimine (two-electron oxidation) product which is electroactive and stable at acidic pH. The intensity of produced yellow colored complex solution can be quantified via UV−vis (semi-quantitative, colorimetry) and current density by electrochemical readout. [38] The electrochemical responses in Fig. 2B showed that, 12.3 μA cm^{-2} current was generated from

the positive sample which is more than 45 times higher than negative control (0.273 μA cm^{-2}). These experimental outcomes from the naked eye observation, colorimetric and amperometric readouts clearly confirmed the peroxidase-like properties of this MIO. The molecular mechanism responsible for the MIO peroxidase mimetics could be followed by the well-established Fenton reaction mechanism, where ferric ions (from porous Fe_2O_3) initiate the reaction through the dissociation of hydrogen peroxide to form free-radical (.OH).[39, 40] The free radical subsequently oxidise the TMB.

To estimate the apparent steady-state kinetics, a range of different concentration of TMB and H_2O_2 were used. The experiments were conducted under the condition (NaAc buffer, pH 3.5, room temperature) followed by our previous report. [37] In this assay, we have optimised the amount of mesoporous materials required and conducted the experiment over a range of MIO (100 ng to 10 μg). It was observed (Fig. S3A), a very less intense color appeared for 200 ng of MIO and increased with increasing MIO quantity. From the corresponding absorbance readout (Fig. S3B), 5 μg and 10 μg of MIO (0.56 vs 0.61) shows almost similar responses (abs@452nm). Thus, we have chosen 5 μg of MIO as optimum for subsequent reaction. Initial rate method was used to evaluate the kinetic parameters of the oxidation reaction. Fig. 2C and 2D show a typical Michaelis−Menten like curves obtained from the suitable concentration range for the both H_2O_2 and TMB, respectively. The data were fitted to the Michaelis–Menten kinetic model using a nonlinear least square fitting routine to obtain the catalytic parameters given in Table S1 and compared with that for previously reported various Iron oxide nanomaterials. All these parameters were also evaluated from the Lineweaver–Burk double-reciprocal plot (1/V vs. 1/S), which gave analogous values (insets of Fig. 2C and D). The apparent K_m value for MIO with TMB was lower than that with HRP, suggesting that the mesoporous MIO have higher affinity with TMB in comparison to the HRP. Moreover, the K_m value of TMB for MIO is also lower than

that of nonporous Iron oxide MIO. This enhanced peroxidase activity of our mesoporous MIO can be explained by the high porosity of the ferric oxide moiety with high surface area [exposure of more Fe(III) ions] and large pore volume that facilitates the increased mass transfer as well as enhances the kinetics of the reaction. Moreover, transfer of lone-pairs electron density (charge transfer) from the amino group of TMB to the vacant d orbital of Fe^{3+} may also enhance the electron density and mobility of Fe_2O_3. [41]

3.3 Colorimetric and amperometric detection of global DNA methylation

Fig. 3 schematically represents the steps involved in the assay design for analysing global DNA methylation in colorectal cancer. In this study, 5mC antibody was used to selectively recognise the methylated cytosine in the ssDNA sequence. Although MBD has also been used to bind with methylcytosine group, it is limited from the requirement of restriction enzymes and cannot effectively bind ssDNA. [42] We have chosen 5mC antibody as it can selectively recognise and bind methylcytosine group in any CpG region. In this assay, genomic DNA were extracted and purified from colorectal cell lines (see the Experimental section for details) followed by denaturation (at 95 °C for 10 min) to generate ssDNA. Previously, we and others have successfully demonstrated that DNA has a specific affinity towards the gold surface through the conventional physisorption and chemisorption mechanism. [43, 44] Thus, the denatured ssDNA samples were directly adsorbed on the SPGE for 10 min. The MIO-5mC antibody was then incubated for 30 min on the SPGE for recognizing methylated DNA. After removing the unbound MIO-5mC antibody conjugates *via* a washing step, TMB substrate solution was added on the electrode surface. The surface-bound MIO catalyses the oxidation of TMB that generates a blue-colored complex, which turns yellow after the addition of an acid solution to the reaction media. The intensity of the colored product is directly proportional to the amount of the captured MIO-mC antibody conjugates, which is, in turn, proportional to the level of methylation present in the sample.

As TMB is electroactive, the amount of enzymatically generated TMB_{ox} was measured chronoamperometrically by applying the potential of +150 mV onto SPGE.

3.4 Assay specificity

To demonstrate the specificity and applicability, we performed our assay using both 5mC antibody specific positive (Jurkat) and negative (WGA) samples. As can be seen in Fig. 4A, an eight times higher absorbance (abs@452 nm) was observed for Jurkat compared to that of WGA (0.498 vs. 0.061). Similar response was also obtained from electrochemical readout (3.234 vs. 0.414 μA cm^{-2}) (Fig. 4B). For further specificity investigation, we also carried out two additional sets of experiment where only PBS was used instead of target DNA (referred as NoT) and a positive sample with 5mC antibody in absence of Fe_2O_3 (referred as control). Both the NoT and control showed negligible response in both colorimetric and electrochemical measurements. However, NoT exhibited slightly higher response than that of control (0.018 vs. 0.014 for abs@452nm). This may be due to the non-specific absorption of MIO at the surface. All these observation clearly demonstrated the good level of specificity of our assay toward the detection of DNA methylation with negligible background using methyl-group specific 5mC antibody.

3.5 Assay optimization

To obtain the sensitive detection, several experimental conditions such as adsorption time, solution pH, DNA and antibody concentration, and incubation time have to be considered and precisely optimized. Previously, we have optimised the several adsorption parameters such as adsorption time, pH of the solution and amount of input DNA to obtain the highest difference between the electrochemical responses of methylated and unmethylated DNA targets. [23, 43, 45] In the current assay, we have adopted all of these optimised parameters (unless otherwise

stated) and used 50 ng of DNA (diluted in 5x SSC buffer, pH 7.4) as an optimum DNA quantity to be adsorbed onto the bare SPGE for 10 min. Another critical measures in our assay is the immunorecognition events of methylated CpG sites by the 5mC antibody. Therefore, the amount of antibody in MIO-5mC antibody conjugates is required to be optimised. Colorimetric absorbance and chronoamperometric current densities were recorded for a series of 5mC antibody concentrations (10 – 100 ng/μL) with a fixed amount of MIO (5 μg of Fe_2O_3). An increasing trend (color intensity) was observed with the increasing of antibody concentration. As shown in Fig. S4A, 75.0 ng/μL and 100.0 ng/μL of antibody produced significantly higher response compared to others. Notably, the current density obtained for 75 ng/μL of antibody was found to be very similar to 100 ng/μL. Thus, 75 ng/μL was selected as the optimal antibody concentration for our assay. We have also optimised the incubation time required for the antibody to achieve the maximum relative absorbance or current density difference between methylated and unmethylated samples. As can be seen in Fig. S4C, 10 mins of 75 ng/μL antibody can show negligible color response for the positive sample. However, from the both colorimetric and amperometric readouts, 30 mins could be the optimised incubation time for this assay as after 45 mins the responses are almost same. Therefore, we have choosen 75 ng/μL of 5mC (for conjugation with MIO) antibody and 30 mins incubation time throughout the assay.

3.6 DNA methylation analysis in heterogeneous samples

We have tested the applicability of our assay to analyse DNA methylation in complex biological samples as the accurate quantification of heterogeneous genome-wide DNA methylation could have significant implications for the prediction of clinical diagnosis and prognosis in human cancers. To examine the heterogeneity at the genome-wide DNA methylation level, a series of heterogeneous samples were prepared by mixing different stoichiometry of Jurkat (100%) and WGA (0%) DNA sequences to get 0%, 10%, 25%, 50%,

75%, 90%, and 100% methylated samples. We observed an increasing trend of color (blue) with increasing methylation level (Fig. 5A). This is because the color intensity obtained by the MIO (from MIO-5mC conjugates) catalysed oxidation, is directly related to the amount of 5mC antibody as well as the amount of 5mC sites on to the electrode surface. It is also noticeable that the color changes related to 0% methylation (almost transparent) was clearly discernible from that of 10% methylated sample (light blue) which confirm the detection limit of our assay by naked-eye evaluation is as low as 10% differences in methylation level.

As can be seen from Fig. 5C, a linear increment with the increasing level of methylation was observed in the UV-Vis absorbance (Abs) measurements, which is fitted with a linear curve with the linear regression equation of y (Abs@450nm) = 0.08 x (% of methylation) + 0.04 with a correction coefficient (R^2) of 0.986. From the colorimetric responses, the limit of detection (LOD) was estimated to be as low as 10% of methylation (Abs 0.81 @452nm). Similarly, the linear regression equation for amperometric readout was estimated as y = 0.03 x + 0.26, with the R^2 of 0.99, confirming the assay sensitivity (LOD of 10%, Fig. 6D). A relative standard deviation (% RSD) for three independent measurements was estimated to be <5.0%, suggesting the good reproducibility of assay toward methylation level detection and quantification. This level of LOD and reproducibility of our colorimetric and electrochemical assay over a wide range of methylation level with low DNA input (total input 50 ng) clearly demonstrates that the peroxidase-like activity of MIO can potentially detect as low as 10% methylation in complex DNA samples. Moreover, we have also compared the performances of our system with that of the HRP/H_2O_2 system. As can be seen from Figure S5, the low detection limit for the HRP/H_2O_2 system was found to be 5% methylation, while it was 10% methylation for the MIO/H_2O_2 system. Although the sensitivity of our method is poorer than that of the HRP/H_2O_2 system, it offers several advantages. Peroxidase-like activity of ferric oxides offers a highly inexpensive alternative of

the natural peroxidase (i.e., HRP), resulting the reduction of cost burden, sophisticated enzyme operation, and open a new window of MIO towards the development of naked-eye and electrochemical DNA methylation assay.

3.7 DNA methylation in cell line

In order to demonstrate the applicability of our assay in more complex biological system, we extended our assay for detecting genome-wide DNA methylation in different colorectal cell lines (HCT-116, SW-48 and FCH-N) samples. The methylation level of these cell lines were compared with both Jurkat and WGA. Fig. 6C and D showed that, the HCT-116 (cancerous) possessed higher methylation level (around 84%) compare to that of WGA and other cell lines which also support by previously published data. [46] On the other hand, both the colorimetric and amperometric responses for a healthy cell line (FCH-N) has relatively lower methylation level (about 18% of methylation) compare to Jurkat and other two cell lines. This finding is completely in agreement with the existing literature. [47] However, our assay has proven to detect methylation level in both synthetic and cell line samples sensitively and specifically; an in-depth study is still needed to evaluate the clinical samples which is outside the scope of this report. Nonetheless, these results here demonstrate the ability to detect as low as 10% of methylation in genomic DNA sequence from minimum of 50 ng of input DNA. Bisulfite and PCR free approaches could reduce the assay time which can be an additional benefit of this assay. Finally, MIO gave more freedom to avoid expensive HRP enzyme, could be a key point to design low cost cancer specific device.

The naked-eye discrimination of the DNA methylation analysis outlined here holds significant potential for the development of inexpensive and user-friendly biosensors in resource-limited settings. In particular, this approach can be exploited as a rapid first-pass

screening (yes/no) tool to analyse the methylation in a large population of DNA samples followed by more sensitive and accurate quantification of methylation *via* chronoamperometric readout. The use of a disposable SPGE effectively eradicates the need of an electrode cleaning process (time-consuming and environmentally unfriendly) typically used in conventional disk electrodes. More importantly, the assay replaces natural enzymes for TMB oxidation, and thus reduces the cost, handling, and storage facilities generally required for natural enzymes. Overall, the assay platform is relatively inexpensive, PCR amplification and bisulfite treatment free, portable and rely on less DNA input.

4. Conclusions

We have successfully investigated the peroxidase mimetic activity of in-house synthesized of a mesoporous iron oxide MIO followed by the development of a simple, low-cost proof-of-concept assay for the detection of global DNA methylation in colorectal cancer cell lines. This MIO showed superior peroxidase mimetic activity compare to other Fe_2O_3 due to their unique morphology and porous structure. The successful replacement of HRP enzyme with MIO enabled us to detect as low as 10% of methylation in the complex synthetic samples with good reproducibility (% RSD = <5%, n = 3) from 50 ng of input DNA. As our assay does not require *(i)* bisulfite treatment, *(ii)* PCR amplification, *(iii)* high DNA input and *(iv)* expensive HRP enzyme (replaced by MIO), it paved the new way to develop a relatively simpler and inexpensive method for DNA methylation detection. Taken these benefits, we anticipate that this peroxidase-mimetics of mesoporous iron oxide and their subsequent application for DNA methylation analysis may opened the new prospect in detecting human cancers or chronic disease.

Conflicts of interest

There are no conflicts to declare.

Acknowledgments

This work was supported by the NHMRC CDF (APP1088966) to M.J.A.S. and HDR scholarships to R.B from Griffith University. This work was partly supported by an Australian Research Council (ARC) Future Fellow (FT150100479) and JSPS KAKENHI Grant Number 17H05393 (Coordination Asymmetry). The authors extend their appreciation to the International Scientific Partnership Program (ISPP) at King Saud University (KSU) for funding this research work through ISPP-0097.

Appendix A. Supplementary material (ESI)

Notes and references

1. S. Zhang, R. Geryak, J. Geldmeier, S. Kim and V. V. Tsukruk, *Chem. Rev.*, 2017, **117**, 12942-13038.
2. V. Urbanova, M. Magro, A. Gedanken, D. Baratella, F. Vianello and R. Zboril, *Chem. Mater.*, 2014, **26**, 6653-6673.
3. S. Yadav, M. K. Masud, M. N. Islam, V. Gopalan, A. K. Lam, S. Tanaka, N. T. Nguyen, M. S. A. Hossain, C. Li, M. Y. Yamauchi and M. J. A. Shiddiky, *Nanoscale*, 2017, **9**, 8805-8814.
4. J. Xie, X. Zhang, H. Wang, H. Zheng, Y. Huang and J. Xie, *Trends Anal. Chem.*, 2012, **39**, 114-129.
5. L. Gao, J. Zhuang, L. Nie, J. Zhang, Y. Zhang, N. Gu, T. Wang, J. Feng, D. Yang, S. Perrett and X. Yan, *Nat. Nanotechnol.*, 2007, **2**, 577-583.
6. H. Wei and E. Wang, *Chem. Soc. Rev.*, 2013, **42**, 6060-6093.
7. Y. Fan, W. Shi, X. Zhang and Y. Huang, *J. Mater. Chem. A,* 2014, **2**, 2482-2486.
8. W. Shi, X. Zhang, S. He and Y. Huang, *Chem. Commun.*, 2011, **47**, 10785-10787.

9. L. Gao, K. Fan and X. Yan, *Theranostics*, 2017, **7**, 3207-3227.
10. E. J. Wee, T. H. Ngo and M. Trau, *Clin. Epigenetics*, 2015, **7**, 65.
11. M. K. Masud, M. N. Islam, M. H. Haque, S. Tanaka, V. Gopalan, G. Alici, N. T. Nguyen, A. K. Lam, M. S. A. Hossain, Y. Yamauchi and M. J. A. Shiddiky, *Chem. Commun.*, 2017, **53**, 8231-8234.
12. S. Liu, F. Lu, R. Xing and J. J. Zhu, *Chemistry*, 2011, **17**, 620-625.
13. K. D. Robertson, *Nat. Rev. Genet.*, 2005, **6**, 597-610.
14. M. Ehrlich, *Oncogene*, 2002, **21**, 5400-5413.
15. A. Aggerholm, P. Guldberg, M. Hokland and P. Hokland, *Cancer Res.*, 1999, **59**, 436-441.
16. K. C. Kuo, R. A. McCune, C. W. Gehrke, R. Midgett and M. Ehrlich, *Nucleic Acids Res.*, 1980, **8**, 4763-4776.
17. J. Singer, W. C. Schnute, J. E. Shively, C. W. Todd and A. D. Riggs, *Anal. Biochem.*, 1979, **94**, 297-301.
18. P. W. Laird, *Hum. Mol. Genet.*, 2005, **14 Spec No 1**, R65-76.
19. S. Lisanti, W. A. Omar, B. Tomaszewski, S. De Prins, G. Jacobs, G. Koppen, J. C. Mathers and S. A. Langie, *PLoS One*, 2013, **8**, e79044.
20. M. N. Islam, S. Yadav, M. H. Haque, A. Munaz, F. Islam, M. S. A. Hossain, V. Gopalan, A. K. Lam, N. T. Nguyen and M. J. A. Shiddiky, *Biosens. Bioelectron.*, 2017, **92**, 668-678.
21. T. Hossain, G. Mahmudunnabi, M. K. Masud, M. N. Islam, L. Ooi, K. Konstantinov, M. S. A. Hossain, B. Martinac, G. Alici, N. T. Nguyen and M. J. A. Shiddiky, *Biosens. Bioelectron.*, 2017, **94**, 63-73.
22. S. O. Kelley, C. A. Mirkin, D. R. Walt, R. F. Ismagilov, M. Toner and E. H. Sargent, *Nat. Nanotechnol.*, 2014, **9**, 969-980.
23. M. H. Haque, R. Bhattacharjee, M. N. Islam, V. Gopalan, N. T. Nguyen, A. K. Lam and M. J. A. Shiddiky, *Analyst*, 2017, **142**, 1900-1908.
24. S. Tanaka, Y. V. Kaneti, R. Bhattacharjee, M. N. Islam, R. Nakahata, N. Abdullah, S. I. Yusa, N. T. Nguyen, M. J. A. Shiddiky, Y. Yamauchi and M. S. A. Hossain, *ACS Appl. Mater. Interfaces*, 2018, **10**, 1039-1049.
25. A. L. N. Lehninger, D. L.; Cox, M. M., *Lehninger Principles of Biochemistry*, W. H. Freeman and Company, 2005.
26. M. Yu, S. Huang, K. J. Yu and A. M. Clyne, *Int. J. Mol. Sci.*, 2012, **13**, 5554-5570.
27. M. C. Bautista, O. Bomati-Miguel, X. Zhao, M. P. Morales, T. González-Carreño, R. P. d. Alejo, J. Ruiz-Cabello and S. Veintemillas-Verdaguer, *Nanotechnology*, 2004, **15**, S154-S159.
28. M. P. M. P. Tartaj, S. Veintemillas-Verdaguer, T. Gonzalez-Carreno, C.J. and Serna, *Synthesis, properties and biomedical applications of magnetic nanoparticles*, Elsevier, Amsterdam, Netherlands, 2006.

29. Y. Jia and J. Li, *Chem. Rev.*, 2015, **115**, 1597-1621.
30. G. T. Hermanson, Bioconjugate Techniques (Third edition), Acedimic press, 2013, http://dx.doi.org/10.1016/B978-0-12-382239-0.00020-0
31. S. Lou, J. Y. Ye, K. Q. Li and A. Wu, *Analyst*, 2012, **137**, 1174-1181.
32. M. Yüce and H. Kurt, *RSC Adv.*, 2017, **7**, 49386-49403.
33. T. E. P. David Josephy, and Ronald P. Mason, *J. Biol. Chem.,* 1982, **257**, 3669-3675.
34. H. Mao, X. Qiu, D. Li, Y. Lin, X. Liu and J. Li, *J. Chem.*, 2015, **2015**, 1-9.
35. R. K. Sahu, D. Mukherjee, J. P. Tiwari, T. Mishra, S. K. Roy and L. C. Pathak, *J. Mater. Chem.*, 2009, **19**, 6810.
36. J. A. Ramos Guivar, E. A. Sanches, F. Bruns, E. Sadrollahi, M. A. Morales, E. O. López and F. J. Litterst, *Appl. Surf. Sci.,* 2016, **389**, 721-734.
37. M. K. Masud, S. Yadav, M. N. Islam, N. T. Nguyen, C. Salomon, R. Kline, H. R. Alamri, Z. A. Alothman, Y. Yamauchi, M. S. A. Hossain and M. J. A. Shiddiky, *Anal. Chem.*, 2017, **89**, 11005-11013.
38. P. D. Josephy, T. Eling and R. P. Mason, *J. Biol. Chem.*, 1982, **257**, 3669-3675.
39. Z. Chen, J. J. Yin, Y. T. Zhou, Y. Zhang, L. Song, M. Song, S. Hu and N. Gu, *ACS Nano*, 2012, **6**, 4001-4012.
40. J. F. Perez-Benito, *J. Phys. Chem. A*, 2004, **108**, 4853-4858.
41. Z. Xing, J. Tian, A. M. Asiri, A. H. Qusti, A. O. Al-Youbi and X. Sun, *Biosens. Bioelectron.*, 2014, **52**, 452-457.
42. T. Kurinomaru and R. Kurita, *Anal. Methods*, 2017, **9**, 1537-1549.
43. A. A. Sina, L. G. Carrascosa, R. Palanisamy, S. Rauf, M. J. A. Shiddiky and M. Trau, *Anal. Chem.*, 2014, **86**, 10179-10185.
44. K. M. Koo, A. A. I. Sina, L. G. Carrascosa, M. J. A. Shiddiky and M. Trau, *Anal. Methods*, 2015, **7**, 7042-7054.
45. K. M. Koo, A. A. Sina, L. G. Carrascosa, M. J. A. Shiddiky and M. Trau, *Analyst*, 2014, **139**, 6178-6184.
46. M. M. Pao, G. Liang, Y. C. Tsai, Z. Xiong, P. W. Laird and P. A. Jones, *Oncogene*, 2000, **19**, 943-952.
47. A. S. Yang, M. R. Estecio, K. Doshi, Y. Kondo, E. H. Tajara and J. P. Issa, *Nucleic Acids Res.*, 2004, **32**, e38.

FIGURE CAPTIONS

Figure 1. (A) SEM image of as synthesized mesoporous iron oxide; (B) a typical TEM image; (C) selected area electron diffraction (SAED) pattern, and (D) high resolution TEM (HRTEM) image.

Figure 2. Mean value response of (B) Absorbance (UV-vis) and (C) amperometric current density for the negative (no MIO) and positive (with MIO) samples (Insets Figure B and C represent corresponding naked eye evaluation and *i-t* curves, respectively). Steady-state kinetic analyses using the Michaelis−Menten model (main) and Lineweaver−Burk model (inset) for the Fe_2O_3 by varying the concentrations of (C) H_2O_2 (0.01−1 M) and (D) TMB (0.01−1.0 mM) with fixed amounts of (C) TMB (800 μM) and (D) H_2O_2 (700 mM), respectively.

Figure 3. Schematic representation of the assay to detect global DNA methylation. Left side represent the DNA preparation steps and right side represent the detection part. Initially, cell lines were grown and extracted using commercial kit. Then, denatured ssDNA was adsorbed onto a SPGE surface followed by immunorecognition of methylated DNA using the MIO-5mC antibody. Subsequent detection of the genomic DNA methylation pattern was performed through coupling reaction of Fe_2O_3 with the TMB/H_2O_2 complex on the SPGE

surface via naked-eye, UV-vis and chronoamperometry. Inset: Typical reaction mechanism for MIO functionalization and 5mC antibody conjugation.

Figure 4. Mean responses of (A) Absorbance and (B) Steady-state amperometric current generated for the assay with one positive (presence of methylated DNA) and with three negative control samples (WGA represents the unmethylated sample, NoT represents PBS instead of positive sample, control represents without DNA and Fe_2O_3-5mC antibodies). Insets: corresponding photos for the naked-eye evaluation and $i-t$ curves.

Figure 5. Detection of DNA methylation in heterogeneous samples. (A) shows the corresponding photos of heterogeneous sample containing 0%, 10%, 25%, 50%, 75%, 90% and 100% methylation and (B) shows chronoamperograms response. Calibration plots obtained for corresponding methylated samples and their mean values of (C) absorbance (UV-vis) and (D) chronoamperometric current density. Each data points in (A) and (C) represents the average of three repeated trials, and error bars represent the standard deviation of measurements within experiments (%RSD = <5%, for n = 3).

Figure 6. (A) Shows representative photos for the naked-eye detection of the methylated genomic DNA (JURKAT), colorectal cancer cell lines (SW-48, HCT-116, FCH-N) and WGA samples. Mean values of (C) absorbance (UV-vis) and (D) chronoamperometric current density for corresponding samples. (B) shows the chronoamperometric response for corresponding cell line samples. Each data point in (C) and (D) represents the average of three repeated trials, and error bars represent the standard deviation of measurements (%RSD =<5%, for n = 3).

FIGURES

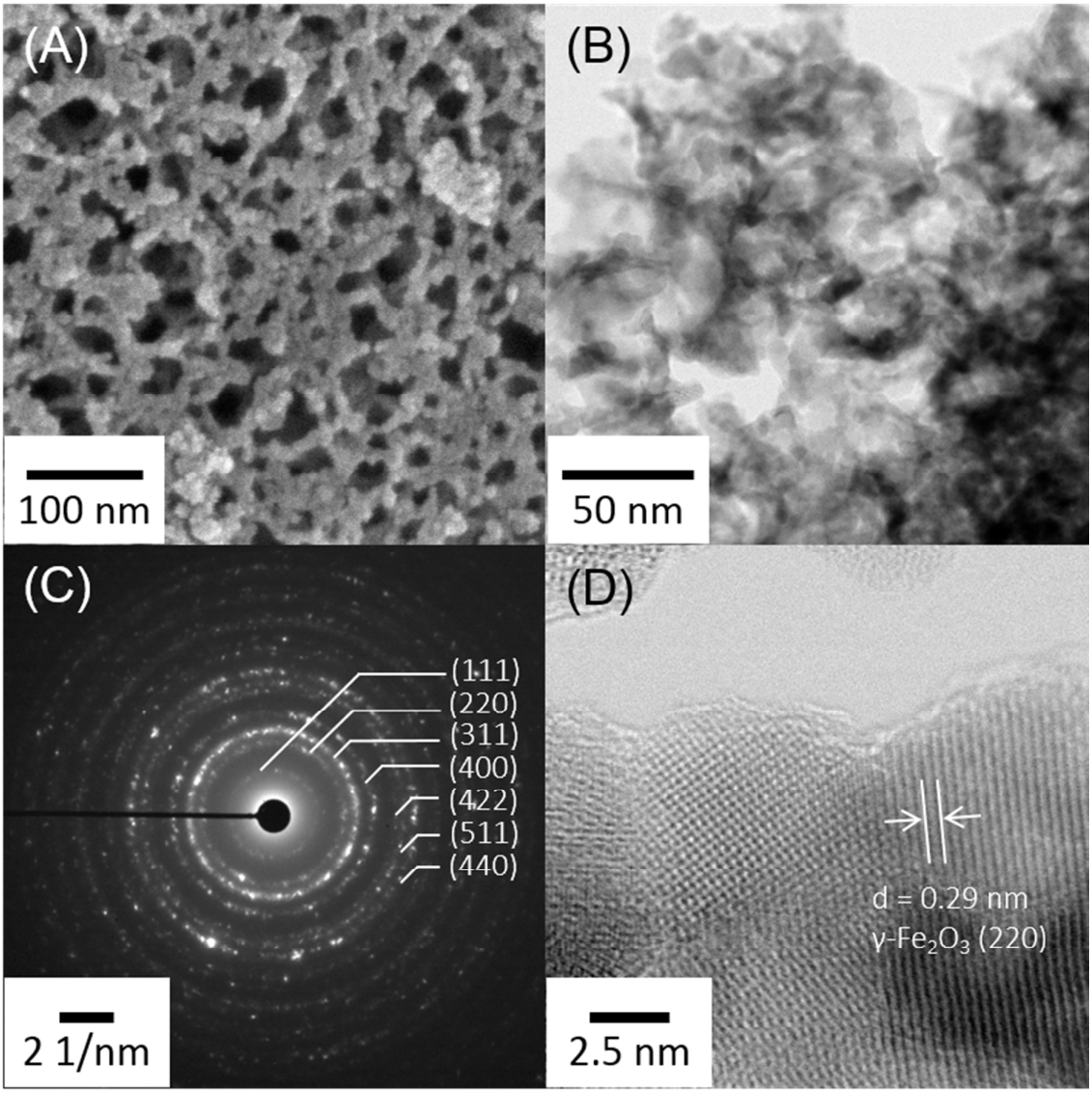
(A)
100 nm
(B)
50 nm
(C)
(111)
(220)
(311)
(400)
(422)
(511)
(440)
2 1/nm
(D)
d = 0.29 nm
γ-Fe2O3 (220)
2.5 nm

Fig. 1.

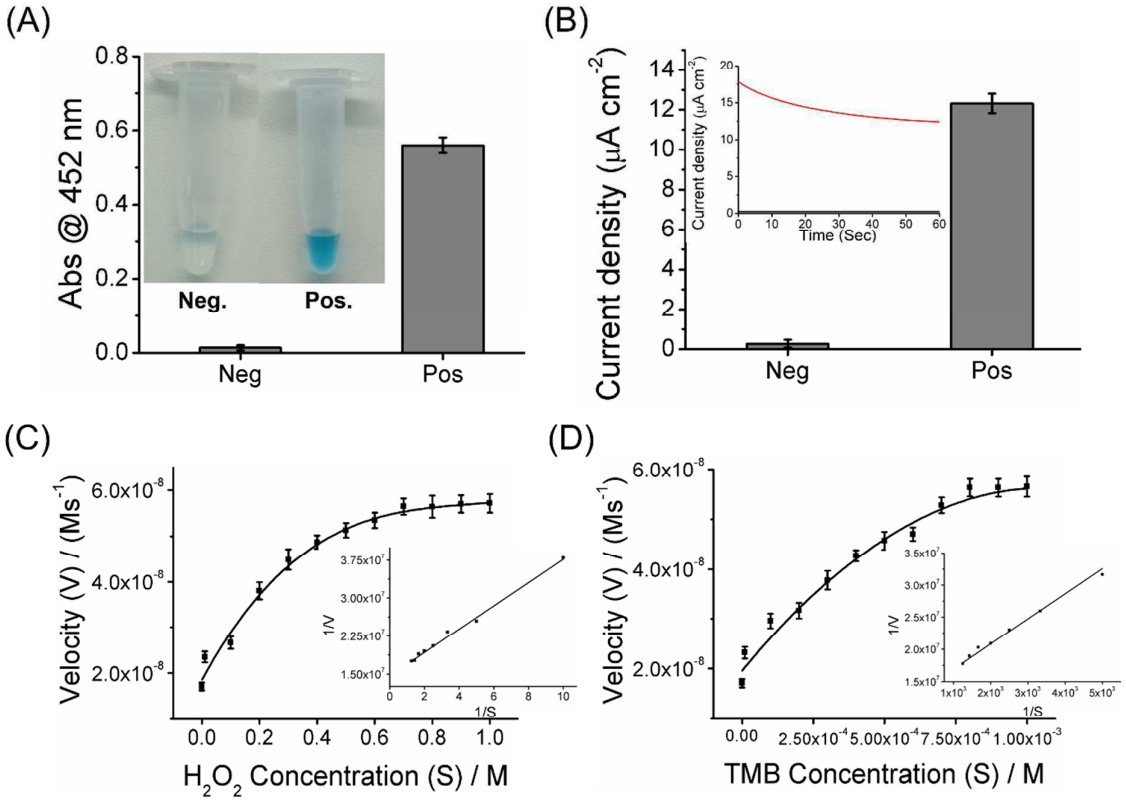
(A)
Abs @ 452 nm
Neg.
Pos.
Neg
Pos
(B)
Current density (μA cm-2)
Current density (μA cm-2)
Time (Sec)
Neg
Pos
(C)
Velocity (V) / (Ms-1)
1/V
1/S
H2O2 Concentration (S) / M
(D)
Velocity (V) / (Ms-1)
1/V
1/S
TMB Concentration (S) / M

Fig. 2.

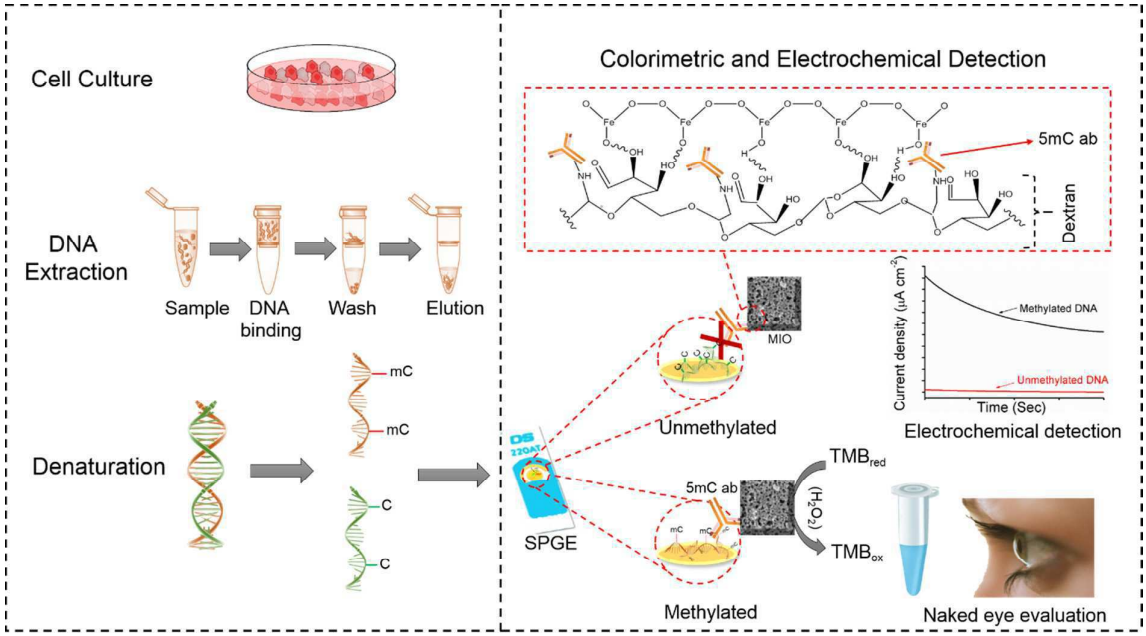
Cell Culture
DNA Extraction
Sample
DNA binding
Wash
Elution
Denaturation
mC
mC
C
C
Colorimetric and Electrochemical Detection
5mC ab
Dextran
MIO
Unmethylated
SPGE
5mC ab
Methylated
TMB$_{red}$
TMB$_{ox}$
(H_2O_2)
Current density (μA cm^{-2})
Methylated DNA
Unmethylated DNA
Time (Sec)
Electrochemical detection
Naked eye evaluation

Fig. 3.

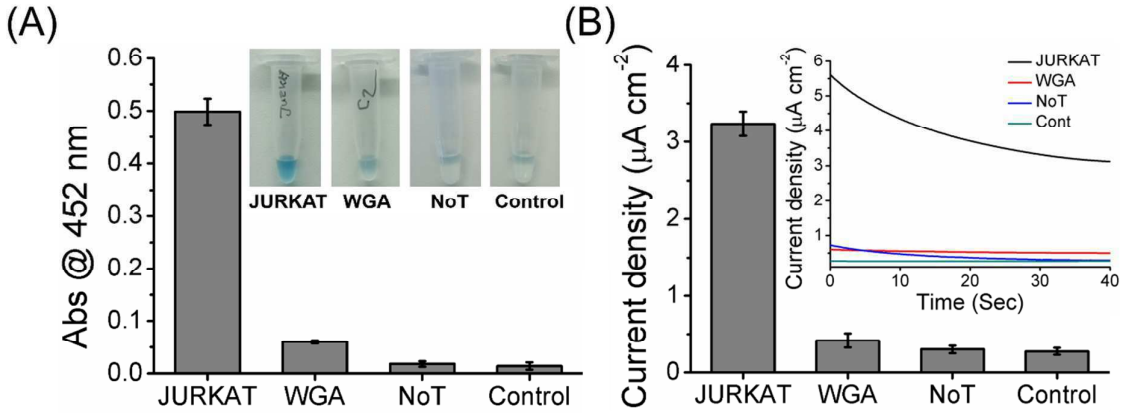
(A)
Abs @ 452 nm
0.6
0.5
0.4
0.3
0.2
0.1
0.0
JURKAT
WGA
NoT
Control
(B)
Current density (μA cm-2)
4
3
2
1
0
JURKAT
WGA
NoT
Control
Current density (μA cm-2)
6
5
4
3
2
1
0
10
20
30
40
Time (Sec)
JURKAT
WGA
NoT
Cont

Fig. 4.

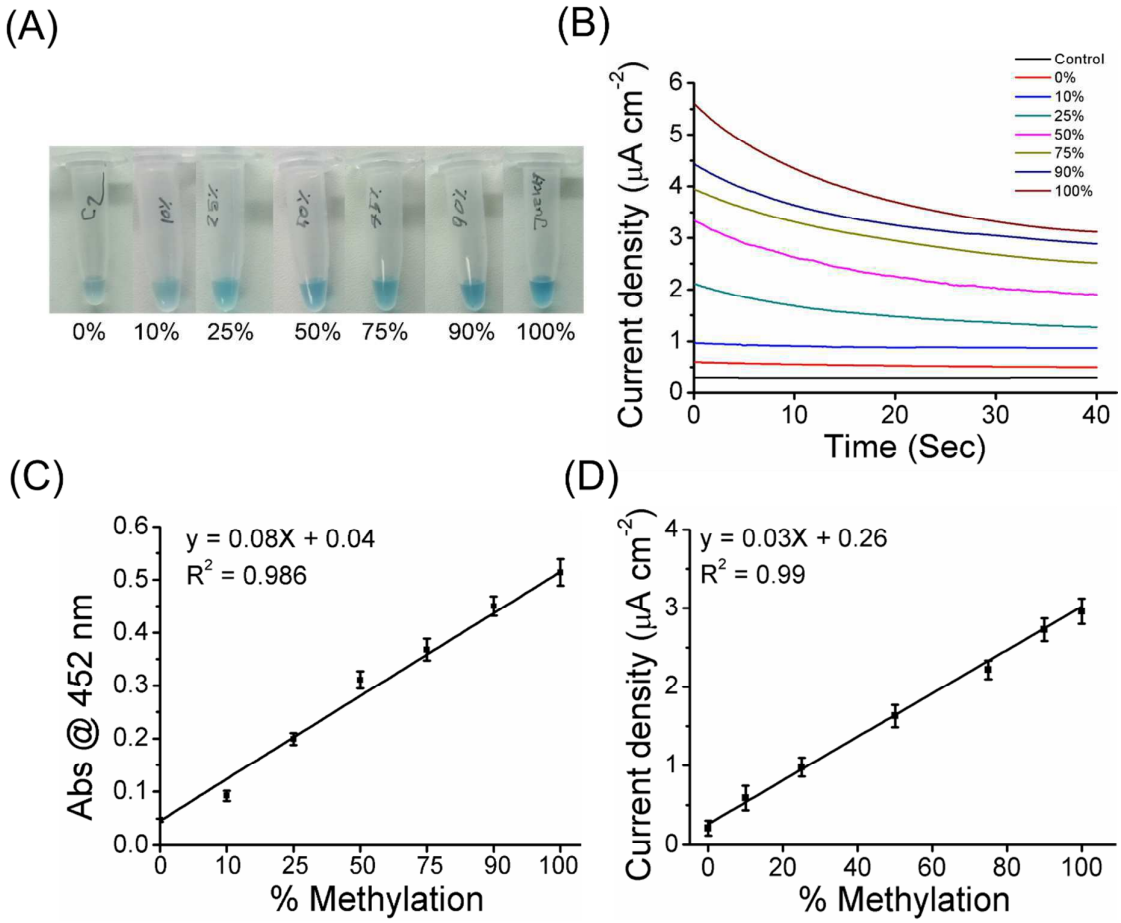
(A)
0%
10%
25%
50%
75%
90%
100%
(B)
Control
0%
10%
25%
50%
75%
90%
100%
Current density (μA cm-2)
Time (Sec)
(C)
y = 0.08X + 0.04
R2 = 0.986
Abs @ 452 nm
% Methylation
(D)
y = 0.03X + 0.26
R2 = 0.99
Current density (μA cm-2)
% Methylation

Fig. 5.

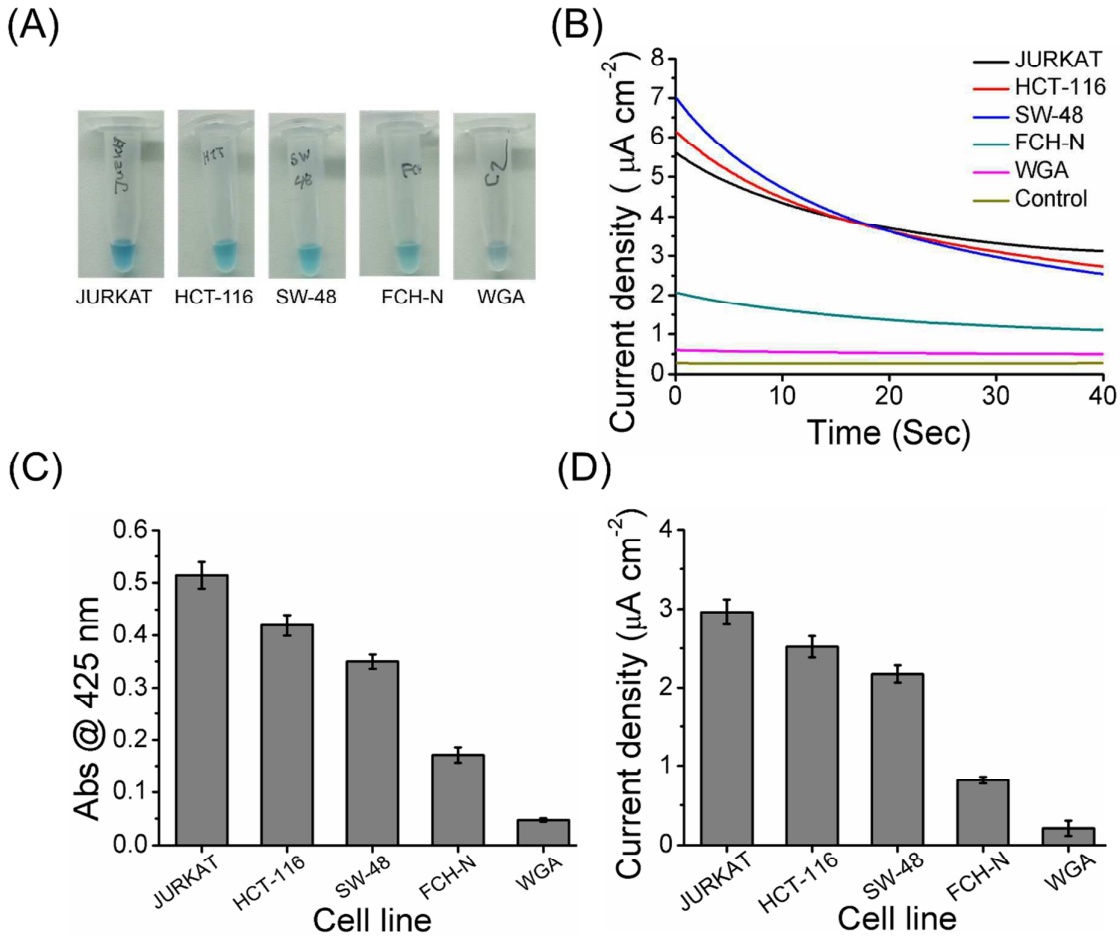
(A)
JURKAT
HCT-116
SW-48
FCH-N
WGA
(B)
Current density (μA cm-2)
Time (Sec)
JURKAT
HCT-116
SW-48
FCH-N
WGA
Control
(C)
Abs @ 425 nm
Cell line
(D)
Current density (μA cm-2)
Cell line

Fig. 6.